

EXGnet: a single-lead explainable-AI guided multiresolution network with train-only quantitative features for trustworthy ECG arrhythmia classification

Tushar Talukder Showrav¹, Soyabul Islam Lincoln²,
Md. Kamrul Hasan^{1*}

¹Department of Electrical and Electronic Engineering, Bangladesh
University of Engineering and Technology (BUET), Dhaka, 1205,
Bangladesh.

²Department of Electronics and Communication Engineering, Khulna
University of Engineering and Technology (KUET), Khulna, 9203,
Bangladesh.

*Corresponding author(s). E-mail(s): khasan@eee.buet.ac.bd;
Contributing authors: 1706087@eee.buet.ac.bd;
islam1709028@stud.kuet.ac.bd;

Abstract

Background: Deep learning has significantly advanced ECG arrhythmia classification, enabling high accuracy in detecting various cardiac conditions. The use of single-lead ECG systems is crucial for portable devices, as they offer convenience and accessibility for continuous monitoring in diverse settings. However, the interpretability and reliability of deep learning models in clinical applications poses challenges due to their black-box nature.

Methods: To address these challenges, we propose EXGnet, a single-lead, trustworthy ECG arrhythmia classification network that integrates multiresolution feature extraction with Explainable Artificial Intelligence (XAI) guidance and train only quantitative features.

Results: Trained on two public datasets, including Chapman and Ningbo, EXGnet demonstrates superior performance through key metrics such as Accuracy, F1-score, Sensitivity, and Specificity. The proposed method achieved average five fold accuracy of 98.762%, and 96.932% and average F1-score of 97.910%, and 95.527% on the Chapman and Ningbo datasets, respectively.

Conclusions: By employing XAI techniques, specifically Grad-CAM, the model provides visual insights into the relevant ECG segments it analyzes, thereby enhancing clinician trust in its predictions. While quantitative features further improve classification performance, they are not required during testing, making the model suitable for real-world applications. Overall, EXGnet not only achieves better classification accuracy but also addresses the critical need for interpretability in deep learning, facilitating broader adoption in portable ECG monitoring.

Keywords: single-lead ECG systems, ECG arrhythmia classification, trustworthy, Explainable Artificial Intelligence, XAI guided, Grad-CAM

1 Introduction

Cardiovascular disease (CVD) is the leading cause of death globally, affecting over half a billion people, with 20.5 million deaths in 2021 [1]. More than 80% of these fatalities result from heart attacks and strokes, with one-third occurring prematurely in individuals under 70 years old [2]. These CVDs can be detected and monitored via various diagnostic tools. One of the most effective is the electrocardiogram (ECG), a fast and simple test that measures heart rate, rhythm, and timing by recording natural electrical impulses in the heart’s various parts [3]. Recent advancements in ECG technology have enabled the developments of portable, cost-effective, and user-friendly devices for point-of-care screening and continuous monitoring. These technologies mostly utilize single-lead ECGs, simplifying the monitoring process of heart activity.

Within the evolving landscape, two main categories of CVD detection technologies that have emerged are traditional methods and deep learning-based methods. Traditional methods comprise of expert features extraction stage and a machine learning algorithm prediction stage. Support vector machine (SVM) classifiers are widely utilized among machine learning methods [4]. Notably, Ye *et.al.*[5] proposed integrating SVM classifiers from ECG samples with wavelet coefficient and RR interval. Discrete wavelet transformation (DWT) was used in early research to extract the QRS wave’s morphological characteristics. Wavelet packet decomposition (WPD) was proposed as an extension to classical DWT because it can only decompose low-frequency components (approximations). This allows both high-frequency and low-frequency components to be used [6]. Chen *et.al.* [7] developed an SVM classifier utilizing RR intervals and ECG projection matrices to classify variable-length ECG signals. Shi *et.al.* [8] used XGBoost algorithms that work with handcraft features to classify ECG, but the model struggled with accurately predicting abnormal classes. Another study incorporated machine learning models including SVM, KNN, and ANN for classification and included parametric features—more precisely, the interval, amplitude, and length of ECG morphology—to improve performance [9]. Cyclic spectral analysis was employed in conjunction with a generalized autoregressive conditional heteroskedasticity model, followed by SVM-based classification, to enhance the analysis of ECG signals by Mihandoost and Amirani [10]. The main drawback of these traditional

methods is that they require hand-crafted features that are dependent on proper ECG signal processing and human intervention. Low-quality or noisy signal fails to provide proper features effectively. Furthermore, experimenting with various feature reduction techniques is essential to identify the optimal set of features.

To overcome these limitations of traditional approaches, deep CNNs have recently gained significant attention from researchers due to their powerful ability to automatically extract and select features directly from input signals. Asgharzadeh *et.al.* [23] proposed calculating spectral entropy to generate a three-dimensional time-frequency transform for QRS complexes and employed bi-directional, two-dimensional PCA to filter out irrelevant features and enhance class separation by simultaneously applying PCA to the rows and columns of the TFT followed by a CNN for classification. Building on this, a novel hidden attention residual network was proposed to extract useful features from ECG signals by converting 2s segments into images [13]. Additionally, a lightweight fusing transformer model was introduced to address challenges related to large-scale parameters and performance degradation, further advancing the capabilities of ECG analysis [24]. Tao *et.al.* [25] incorporated an expert-knowledge attention network to recognize four tachyarrhythmias, highlighting the need for deep learning approaches to consider inter-channel shared information and time-sequence dependent signals. In another study [26], a lightweight custom CNN and transfer learning model with MobileNet-V2 architecture was applied to segmented ECG image data that was balanced by auxiliary classifier generative adversarial network (ACGAN). Chen *et.al.* [20] developed an ensemble multiscale CNN with two modules: LSTM network learns from 1-D signals and time-frequency spectrograms from denoised ECG signals on VGGNet. The CWT scalogram from a single-lead ECG signal was employed in a study by Xie *et.al.* [16]. In a different research, spectrograms of 1D-ECG signals were created using the superlet-transform-based (SLT) method as opposed to the CWT and ResNet-18 for classification [17]. Islam *et.al.* [27] proposed an attention, convolution, and transformer-based network, to effectively capture heartbeat morphological characteristics using peak annotation on ECG signals incorporating preprocessing algorithms like synthetic minority oversampling technique edited nearest neighbor (SMOTE-ENN), SMOTE-Tomek, and adaptive synthetic. On another approach, a novel inter-patient heartbeat classification model, G2-ResNeXt, was proposed to enhance the recognition of patient's heart conditions by incorporating a two-fold grouping convolution (G2) into the original ResNeXt structure [15]. To tackle class imbalances in ECG data, a context-aware loss was introduced in [18], which dynamically adjusts weights according to class representation.

Explainable artificial intelligence (XAI) methods are relatively new in the field of deep learning-based biomedical signal analysis, with only a few studies exploring various XAI techniques for ECG classification. Jo *et al.* [28] developed a CNN architecture with submodules to detect the presence of P waves and RR irregularities, using gradient class activation maps (Grad-CAM) to interpret the results. Bender *et.al.* [29] employed multiple layer-wise relevance propagation (LRP) rules and integrated gradients (IG) for interpreting different arrhythmias. In contrast, Singh & Sharma [30] performed a more comprehensive comparison of four XAI methods, including Grad-CAM, and Shapley Additive Explanations (SHAP). Goettling *et.al.* [21] compared 13

Table 1 Summary of recent studies on arrhythmia classification using deep learning algorithms.

Author	Year	Class	Approach	Database	Accuracy	Sensitivity	Specificity
Hannun <i>et.al.</i> [11]	2019	AFib-AF, AVB, EAR, IVR, Junctional, Noisy, SR, SVT, VT, Trigeminy, Bigeminy	CNN	(Private)	-	75.22	97.2
Petmezas <i>et.al.</i> [12]	2021	AFib, NSR, AF, J	CNN, LSTM	MIT-BIH	97.4	97.0	98.4
Guan <i>et.al.</i> [13]	2022	SB, SR, SI, AFL, AFib	HA-Resnet	Chapman	88.16	79.08	98.16
Serhal <i>et.al.</i> [14]	2023	AFib, NSR	EMD, CNN	PTB-XL	98.80	-	-
Hao <i>et.al.</i> [15]	2023	SR, SB, ST, AF, AFib, SVT	G2-ResNeXt	Chapman	98.38	97.34	99.59
Xie <i>et.al.</i> [16]	2024	AFib, non-AFib	CWT-MB-ResNet	Physionet	-	-	-
Singhal <i>et.al.</i> [17]	2024	AFib, SR, VF	GSMD-SRST	Physionet, Mendelej	99.20	98.60	99.00
Gais <i>et.al.</i> [18]	2024	N, S, V, F, Q	Bidirectional Transformer	MIT-BIH	94.26	93.15	-
Choi <i>et.al.</i> [19]	2024	AFib, non-AFib	LSTM, XGBoost	PTB-XL, Chapman	93.00	95.35	89.56
Chen <i>et.al.</i> [20]	2024	Normal, AFib, Other, Noisy	EMCNet	Physionet	90.50	85.00	92.00
Goettling <i>et.al.</i> [21]	2024	AFib, non-AFib	xECGArch	PTB-XL, Georgia, CPSC 2018, Chapman	95.33	94.87	95.82
Ayano <i>et.al.</i> [22]	2024	SR, SB, ST, AF-AFib, SVT	CNN-BiLSTM	Chapman	95.81	93.79	98.94

different XAI methods, and among those techniques, the deep Taylor decomposition (DTD) explanation seemed more trusted. H. Le *et.al.* [31] used modified Grad-CAM for lead-wise explanation. They instantiate Spearman’s rank correlation to assess the quality of the XAI approach. In another work, Ayano *et.al.* [22] employed two model interpretability techniques namely, Grad-CAM++ and SHAP. Table 1 contains a brief overview of works along with their corresponding classification performance scores.

Most studies using deep CNNs, RNNs, or hybrid methods have solely trained on raw ECG signals or expert features. However, certain heart arrhythmias have correlations with specific morphological features, making it essential to consider both for accurate interpretation. To improve performance, some studies have integrated these quantitative features with deep learning networks. Besides, in many cases, the visualizations generated by XAI techniques may not align with verbal descriptions used in medical practice and may lack clarity in highlighting key ECG segments. We address these limitations by introducing a novel architecture, EXGnet, which provides a reliable, trustworthy, and interpretable deep learning framework for ECG analysis. Our major contributions are as follows:

- We introduce a novel deep learning architecture that efficiently extracts multiresolution features from ECG signal while minimizing computational complexity. This approach enables the model to learn both short-term and long-term features within a single network.
- We introduce XAI guidance through a Normalized Cross-Correlation (NCC)-based loss function to guide Class Activation Map (CAM) values. This novel approach ensures that our deep learning model focus on the specific regions of ECG signals that cardiologists typically examine for decision-making.
- We strategically integrate quantitative features solely during the training phase of our network, enabling it to leverage these features for robust learning. Notably, during testing, no quantitative features are needed, yet the network delivers improved performance compared to when these features were absent during training.

2 Materials and Methods

2.1 Materials

2.1.1 Datasets

To evaluate the performance of EXGnet, we conducted experiments using the publicly available database from the PhysioNet/Computing in Cardiology Challenge 2021 [32]. This database includes ECG recordings from various challenges and hospitals, totaling 45,512 recordings from the Chapman-Shaoxing [33] (Chapman dataset) and Ningbo [34] datasets, each sampled at 500 Hz for 10 seconds. Both of these datasets are jointly available online in a Physionet official link (<https://physionet.org/content/ecg-arrhythmia/1.0.0/>).

We focused on the following heart conditions: Sinus Rhythm (SR), Sinus Arrhythmia (SA), Sinus Tachycardia (ST), Sinus Bradycardia (SB), Atrial Fibrillation (AFib), Atrial Flutter (AF), Atrial Tachycardia (AT), and Supraventricular Tachycardia (SVT). These were selected for effective identification using the lead II signals. To

enable multiclass classification, we ensured each ECG recording had a unique class, although some signals may belong to multiple categories. This resulted in 5,086 recordings from the Chapman dataset and 16,411 from the Ningbo dataset. Due to insufficient data, we combined AF with AFib and AT with SVT. Besides, research shows that AF and AFib signals are often quite similar in these datasets [35]. The class distribution is detailed in Table 2. Since there are only 15 samples available for the combined AT and SVT class in the Ningbo dataset, we decided to omit this class from our analysis.

Table 2 Class distribution across different datasets

Database	Class					
	SR	SB	ST	SA	AF+AFib	AT+SVT
Chapman	1362	2195	639	0	501	390
Ningbo	4535	6691	2563	1232	1375	15

2.1.2 Quantitative features extraction

In our work, we utilized quantitative features extracted from ECG signals using the NeuroKit 0.2 Python library [36]. This library offers a comprehensive set of functions that can be applied to ECG data to extract essential features, aiding in detailed signal analysis. The following 17 features have been extracted from the ECG signal: beats per minute (BPM), mean of normal-to-normal intervals (Mean NN), standard deviation of successive differences (SDSD), standard deviation of NN intervals (SDNN), and root mean square of successive differences (RMSSD). Additional features include the coefficient of variation of successive differences (CVSD), coefficient of variation of NN intervals (CVNN), median NN intervals (Median NN), median absolute deviation of NN intervals (MAD NN), and the median coefficient of variation of NN intervals (MCV NN). We also extracted the interquartile range of NN intervals (IQR NN), the standard deviation of the RMSSD (SDRMSSD), 20th and 80th percentiles of NN intervals (Prc20 NN, Prc80 NN), minimum NN intervals (Min NN), maximum NN intervals (Max NN), and the heart rate turbulence index (HTI).

2.1.3 Data preprocessing

For preprocessing, we minimized interventions to preserve raw signal characteristics. We applied three median filters with widths of 0.2, 0.6, and 1.2 seconds to the input signal, then subtracted the filtered components from the original signal to emphasize high-frequency details. After denoising, we normalized the signal values to a range of 0 to 1.

To generate the ground truth mask for XAI guidance, we concentrated on RR interval variability. We first calculated all the RR intervals from the ECG signal and then determined the absolute mean difference from the mean RR interval. Using Equation 2, we computed values only when $RR_{intervals}^{difference}$ is greater than or equal to

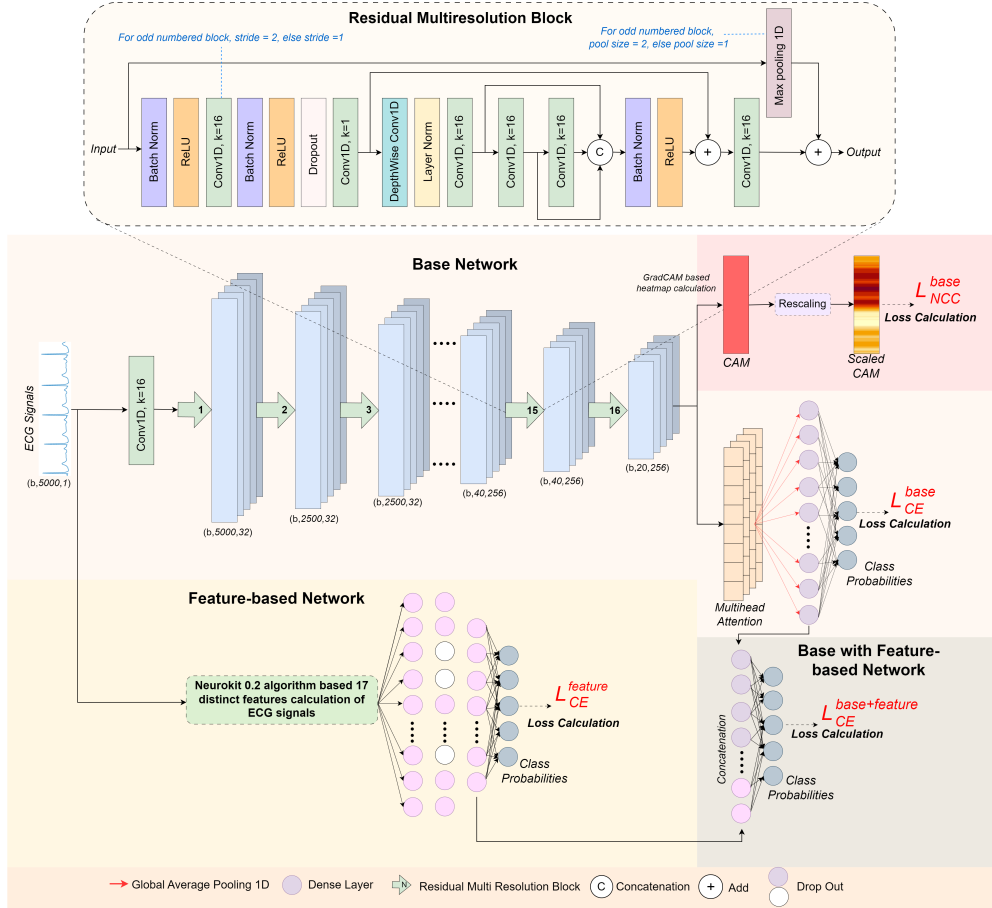


Fig. 2 Detailed block diagram of the proposed EXGnet

to extract and integrate both [21], our design takes a better approach. We introduce a residual multiresolution block that utilizes convolutions with varying kernel sizes and depth-wise convolutions to capture multiresolution features without the need for separate CNNs. To address the computational overhead associated with larger kernels, we draw inspiration from Navid *et.al.* and Showrav *et.al.* [37, 38], implementing a parallel convolutional structure. Here, we use three 16×16 kernel convolutions to get the advantage of both 16×16 , 31×31 , and 46×46 convolutions, thus reducing the computation cost. This design achieves multiresolution feature extraction with reduced computational complexity.

The residual multiresolution block also includes depth-wise convolution, enabling the network to learn features from individual channels. Similar to the work of Hannun *et.al.* [11], we incorporate shortcut connections to facilitate efficient optimization. Our base network comprises 16 residual multiresolution blocks, with every alternate block subsampling its inputs by a factor of two. Corresponding Max Pooling layers within the

blocks also perform subsampling on alternate layers. Batch normalization is applied before each ReLU activation layer, and a Dropout layer is used to mitigate overfitting. The number of channels per multiresolution block begins with 32 and doubles after every four blocks, ending with 256 in the final block.

Following the final residual multiresolution block, Multi-Head Attention is applied with 8 heads and an embedded dimension of 256, followed by a Global Average Pooling (GAP) layer. The network concludes with a Dense layer, the size of which corresponds to the number of arrhythmia classes, using Softmax activation to output the predicted class.

2.2.2 XAI guidance

In deep learning applications for arrhythmia detection, it is crucial to consider not only whether a model accurately predicts the condition but also how we can trust these predictions. Specifically, we need to determine if the results stem from the same regions of ECG signals that cardiologists traditionally rely on for their diagnoses. To address these concerns, XAI techniques can be employed to evaluate the trustworthiness and reliability of the model’s output. Several studies in the literature have used methods such as Grad-CAM and Shapley values to interpret the decisions of neural networks, thereby enhancing confidence in their predictions [21]. However, to the best of our knowledge, no prior studies has investigated the integration of XAI guidance during the training phase.

In this paper, we propose a novel approach that incorporates XAI-guided training. Specifically, we use Grad-CAM [39] within the network to generate CAMs from the output of the final multiresolution block. In our model, the CAM consists of 20 values, each corresponding to a sequential block of 250 samples from the original 5000-sample ECG signal. A CAM value close to 1 indicates that the corresponding region contains features critical to the final prediction. Previous research has shown that many severe heart conditions are associated with significant variability in the RR interval [40]. Therefore, we initially focus on RR interval variability in the ECG signal. To guide the network, we apply a 1D mask of 20 samples long generated by considering the RR intervals provided by the NeuroKit 0.2 algorithm, which is designed to capture heart rate variability. By guiding the network with these masks, the model learns to concentrate on clinically relevant regions of the signal, thereby emulating the decision-making process of a cardiologist.

2.2.3 Train-only quantitative features integration

Machine learning approaches to ECG arrhythmia classification rely on the extraction of various statistical, morphological, and handcrafted features from the ECG signal, followed by the utilization of classifiers such as Random Forest, Gradient Boosting, and Naive Bayes. However, these methods frequently fall short of providing optimal results. To improve performance, some studies have integrated these quantitative features with deep learning networks, yielding better outcomes. Despite these advances, the complexity of calculating numerous features poses a significant challenge for portable ECG devices, where computational efficiency is crucial.

To overcome this limitation, we utilized train-only quantitative features, demonstrating that better results can be achieved also when these features are excluded during testing. In the testing phase, only the raw ECG signal is required, eliminating the computational burden of feature extraction, and making the system more suitable for portable ECG devices. We employ 17 distinct quantitative features, which pass through a tiny, separate network. This network consists of three dense layers, with the final layer’s size corresponding to the number of arrhythmia classes and utilizing Softmax activation. The output of the second dense layer is concatenated with the output of the GAP layer of the base network. The combined output then passes through another dense layer with Softmax activation for final prediction. This strategic use of train-only quantitative features allows the network to learn additional features through a reciprocal loss function, enhancing the overall performance of the model.

2.3 Loss functions

We used Categorical Cross-Entropy (CE) loss during training of the network to learn arrhythmia labels. This can be expressed as

$$L_{CE} = - \sum_{i=1}^N \sum_{c=1}^C y_{i,c} \log(\hat{y}_{i,c}) \quad (3)$$

where, N is the number of samples, C is the number of classes, and $\hat{y}_{i,c}$ is the predicted probability where the ground truth probability is $y_{i,c}$. Besides, to guide the network with XAI, we use Grad-CAM. To guide the CAM values we utilize Normalized Cross Correlation (NCC) loss function, which helps the network to learn making the CAM values orientation as per the ground truth. The NCC loss can be expressed as

$$L_{NCC} = - \frac{1}{N} \sum_{i=1}^N \frac{\sum_{j=1}^M \left(\frac{A_{i,j} - \mu_A}{\sigma_A} \right) \left(\frac{B_{i,j} - \mu_B}{\sigma_B} \right)}{M} \quad (4)$$

where, N is the number of samples, M is the number of values in CAM, and A and B denote the ground truth and prediction, respectively. The total loss function can be written as

$$L_{total} = \alpha \cdot L_{CE}^{base} + \beta \cdot L_{CE}^{feature} + \gamma \cdot L_{CE}^{base+feature} + \delta \cdot L_{NCC}^{base} \quad (5)$$

where, L_{CE}^{base} is the loss function for base network, $L_{CE}^{feature}$ for guiding the train-only quantitative feature based network, $L_{CE}^{base+feature}$ for guiding both base with feature based network, and L_{NCC}^{base} for guiding the CAM values in the base network. In our work, through experimentation we selected α, β, γ and δ values as 2, 1, 1, and 0.2, respectively.

3 Results

3.1 Experimental setup

3.1.1 Implementation details

In this research, we used five-fold cross-validation to evaluate the proposed segmentation network, which was trained with a batch size of 4 on an NVIDIA Tesla P100 PCIe GPU. We utilized the Adam optimizer and the initial learning rate was 0.0002. The networks were trained for up to 200 epochs on the Chapman dataset and 100 epochs on the Ningbo dataset. After the first 60 epochs, we applied a Cosine Annealing learning rate scheduler with an initial learning rate of 0.0001 for 20 epochs. Subsequently, the initial learning rate of the Cosine Annealing scheduler was halved every 40 epochs. We also experimented with various ECG data augmentation techniques to balance the class samples; however, we did not observe any significant impact from these augmentations in our experiments, consequently, we chose not to include them in our final approach.

3.1.2 Evaluation metrics

To evaluate the proposed method and conduct a comparative analysis with the existing literature, we utilized several key performance metrics: Accuracy, F1-score, Sensitivity, and Specificity. Each metric offers distinct insights into the model’s effectiveness. Accuracy quantifies the overall correctness of the model in classifying instances. It is defined as

$$\text{Accuracy} = \frac{TP + TN}{TP + TN + FP + FN} \quad (6)$$

where, TP represents the number of correctly identified positive cases, TN indicates the number of correctly identified negative cases, FP is the number of negative instances incorrectly classified as positive, and FN is the number of positive instances incorrectly classified as negative. The F1-score serves as a harmonic mean of Precision and Recall, providing a balanced measure of a model’s performance, particularly useful in scenarios involving class imbalance. It is calculated as

$$F1\text{-score} = 2 \times \frac{\text{Precision} \times \text{Recall}}{\text{Precision} + \text{Recall}} = \frac{2 \cdot TP}{2 \cdot TP + FP + FN} \quad (7)$$

Sensitivity, also referred to as Recall or True Positive Rate, assesses the model’s ability to correctly identify positive instances. It is defined as

$$\text{Sensitivity} = \frac{TP}{TP + FN} \quad (8)$$

Specificity, or True Negative Rate, measures the model’s capacity to accurately identify negative instances. It is computed as

$$\text{Specificity} = \frac{TN}{TN + FP} \quad (9)$$

By employing these metrics, we gained a comprehensive understanding of the model’s performance and relative efficacy compared to other published works. Each metric highlights different aspects of performance, enabling us to identify strengths and areas for improvement in our approach.

3.2 Performance comparison

Table 3 provides a comprehensive comparison of the proposed networks against the most recent methods on the Chapman and Ningbo datasets. In our proposed method, we can either derive predictions from the base model’s output, which requires no quantitative features during testing, or utilize the combined model’s output when quantitative features are incorporated during inference. To clarify, we refer to the model that uses the combined output as EXGnet-L. Since our primary goal is to avoid using quantitative features during testing, we will concentrate on the output of the base EXGnet.

We employed five-fold cross-validation to evaluate each model, ensuring a thorough and equitable assessment of performance across several metrics, including sensitivity, specificity, accuracy, and F1-score. On the Chapman dataset, EXGnet achieves an impressive average accuracy of 98.762% and an F1-score of 97.910%, surpassing all previously mentioned state-of-the-art models. It consistently performs well across all metrics in each of the five folds, attaining the highest average sensitivity and specificity 97.850% and 99.698%, respectively. Furthermore, when quantitative features are provided during inference, performance improves significantly, with increases of +0.118% in accuracy and +0.285% in F1-score. Among the comparing methods, xECGArch yields the best average accuracy of 98.565% and an F1-score of 97.451%. Notably, xECGArch performs better than EXGnet in fold 3, although our method outperforms it in the other folds. When utilizing the combined model with quantitative features, EXGnet also surpasses xECGArch in fold 3. Additionally, G2-ResNeXt demonstrates compelling performance in fold 4 of the Chapman dataset.

In the Ningbo dataset, there is a slight decline in performance across all models, primarily due to the noisy and more challenging ECG signals. However, our proposed EXGnet consistently outperforms other existing methods across all metrics. As shown in Table 3, EXGnet achieves 96.932% accuracy (+0.250% compared to the second-best model), 95.527% F1-score (+0.546% compared to the second-best model), 95.403% sensitivity (+0.596% compared to the second-best model), and 99.210% specificity (+0.083% compared to the second-best model). Moreover, when quantitative features are provided during testing (EXGnet-L), performance improves significantly ($p < 0.001$), achieving an average accuracy of 97.274% and an F1-score of 96.069%. Among the compared methods, G2-ResNeXt achieves the highest average accuracy at 96.682%, while xECGArch achieves the best F1-score at 94.981%. It is evident from Table 3 that the performance of the Interpretable Multichannel Deep Learning Model is inferior to that of other methods. This may be because this method was designed for classifying twelve-lead ECG signals, and since we applied it to single-lead ECG data, the model may not have adapted well to deliver optimal performance. Overall, the results in Table 3 highlight how effective our proposed models are for single lead ECG arrhythmia classification. Our network consistently achieves better results in key

Table 3 Quantitative comparison of the proposed network with most recent state-of-the-art methods.

Methods	Folds	Chapman			Ningbo		
		Accuracy	F1-score	Specificity	Accuracy	F1-score	Specificity
Interpretable Hybrid Multichannel Deep Learning Model [22]	<i>Fold 1</i>	95.481	93.654	94.248	93.049	87.383	85.630
	<i>Fold 2</i>	95.088	92.657	92.300	89.970	83.024	81.237
	<i>Fold 3</i>	95.379	92.632	93.186	91.552	87.227	85.886
	<i>Fold 4</i>	96.853	95.336	95.724	92.925	86.745	85.591
	<i>Fold 5</i>	96.264	93.991	93.516	89.814	84.025	83.685
	<i>Average</i>	95.813	93.654	93.795	91.462	85.681	84.406
G2-ResNeXt [15]	<i>Fold 1</i>	98.428	97.189	97.237	96.951	94.545	95.209
	<i>Fold 2</i>	97.937	96.342	96.789	96.248	94.895	94.567
	<i>Fold 3</i>	98.132	96.799	96.856	96.279	94.392	93.479
	<i>Fold 4</i>	98.820	98.074	97.977	96.920	95.301	94.351
	<i>Fold 5</i>	98.623	97.947	97.834	97.011	95.535	94.772
	<i>Average</i>	98.388	97.270	97.339	96.682	94.934	94.476
xECGArch [21]	<i>Fold 1</i>	98.723	97.955	97.890	96.646	95.030	95.736
	<i>Fold 2</i>	98.232	96.632	96.413	96.340	95.036	94.715
	<i>Fold 3</i>	98.525	97.328	97.034	96.493	94.751	94.394
	<i>Fold 4</i>	98.722	97.841	97.696	96.950	95.223	95.223
	<i>Fold 5</i>	98.623	97.499	97.275	96.706	94.865	93.968
	<i>Average</i>	98.565	97.451	97.262	96.627	94.981	94.807
EXGnet (Ours)	<i>Fold 1</i>	99.116	98.542	98.430	97.043	95.661	96.023
	<i>Fold 2</i>	98.428	97.043	97.019	96.523	95.082	94.651
	<i>Fold 3</i>	98.427	97.452	97.487	96.859	95.276	94.802
	<i>Fold 4</i>	98.820	98.069	98.055	96.920	95.531	95.354
	<i>Fold 5</i>	99.017	98.443	98.257	97.316	96.085	96.185
	<i>Average</i>	98.762	97.910	97.850	96.932	95.527	95.403
EXGnet-L (Ours)	<i>Fold 1</i>	99.312	98.764	98.617	97.348	96.103	96.327
	<i>Fold 2</i>	98.722	97.974	97.903	97.011	95.875	95.877
	<i>Fold 3</i>	98.623	97.759	97.603	97.133	95.825	95.887
	<i>Fold 4</i>	98.722	97.850	97.764	97.225	96.140	96.109
	<i>Fold 5</i>	99.017	98.628	98.390	97.652	96.402	96.248
	<i>Average</i>	98.880	98.195	98.055	97.274	96.069	96.090

Table 4 Ablation study demonstrating the effect of the newly introduced components in the proposed method.

Methods	Loss			Chapman			Ningbo			
	L_{CE}^b	L_{NCC}^b	$L_{CE}^{b,f}$	Accuracy	$F1$ -score	Sensitivity	Accuracy	$F1$ -score	Sensitivity	
(a) Baseline	✓			97.857	96.286	96.299	99.473	95.822	94.298	93.563
(b) a + Multiresolution	✓			98.525	97.421	97.354	99.631	96.584	95.136	94.270
(c) b + XAI guidance	✓	✓		98.644	97.699	97.665	99.661	96.859	95.362	95.003
(d) b + Quantitative features	✓		✓	98.585	97.528	97.527	99.648	96.828	95.234	95.009
(e) b + c + d (EXGnet)	✓	✓	✓	98.762	97.910	97.850	99.698	96.932	95.527	95.403
(f) b + c + d (EXGnet-L)	✓	✓	✓	98.880	98.195	98.055	99.728	97.274	96.069	96.090

metrics compared to the existing methods. The compelling performance of EXGnet and EXGnet-L proves they can adapt well to different datasets, making them reliable choices for clinical ECG analysis and setting a new benchmark in the field.

4 Discussion

4.1 Ablation study

We conducted a comprehensive ablation study to quantitatively assess the impact of each new component in our proposed method. Table 4 outlines the incremental performance improvements achieved through various configurations: (a) Baseline, (b) Baseline with multiresolution feature extraction, (c) Baseline + multiresolution feature extraction + XAI guidance via Grad-CAM, (d) Baseline + multiresolution feature extraction + quantitative features integration, (e) Baseline + multiresolution feature extraction + XAI guidance + quantitative features integration (results from the base network EXGnet), and (f) Baseline + multiresolution feature extraction + XAI guidance + quantitative features integration (results from the combined network EXGnet-L). We present the ablation study on the both Chapman and Ningbo datasets, with average five fold results evaluated using Accuracy, F1-score, Sensitivity, and Specificity, as shown in Table 4.

As shown in Table 4, the baseline model demonstrated significant performance improvements (p-value < 0.001) with the addition of the multiresolution convolution, yielding increases of 0.668% and 0.762% in accuracy, along with 1.135% and 0.838% in F1-score for the Chapman and Ningbo datasets, respectively. Introducing XAI guidance further enhanced performance, with accuracy and F1-score gains of 0.119% and 0.278% on the Chapman dataset, and 0.275% and 0.226% on the Ningbo dataset. Additionally, incorporating quantitative features alongside the multiresolution block also led to improvements in both datasets (+0.06% and +0.244% in accuracy, and +0.107% and +0.098% in F1-score).

The results clearly indicate that the addition of XAI guidance has a more substantial quantitative impact than integrating quantitative features. However, when both techniques are applied, the accuracy reaches 98.762% and 96.932%, with F1-scores of 97.910% and 95.527% for the Chapman and Ningbo datasets, respectively, without needing quantitative features during testing. Furthermore, when quantitative features are utilized during testing, the combined model (EXGnet-L) outperformed all metrics across both datasets, with increases of +0.118% and +0.342% in accuracy, and +0.285% and +0.542% in F1-score. Notably, even with only XAI guidance or quantitative features integration, our proposed network outperformed the existing state-of-the-art models on both dataset.

4.2 Evaluation of trustworthiness

In the ablation study section, we showed the quantitative impact of incorporating XAI guidance (see Table 4). However, these quantitative results alone do not reveal whether the network’s correct predictions are based on the specific segments of the ECG signal that a cardiologist would typically analyze during detecting arrhythmia.

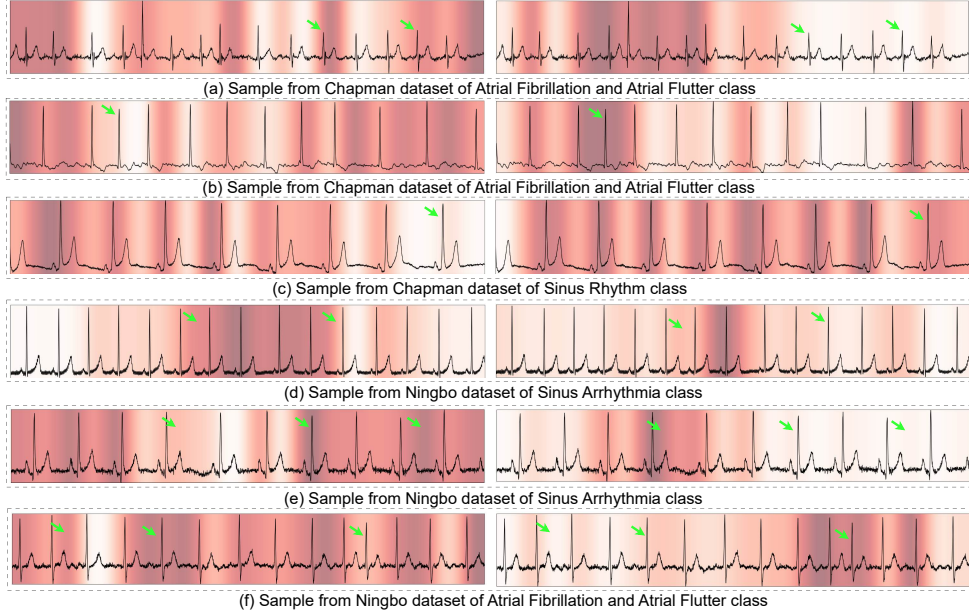


Fig. 3 Visualization of the effect of XAI guidance on the proposed network. The left side shows the CAM outputs from the model without XAI guidance, while the right side displays the outputs when XAI guidance is applied. Green marks indicate the regions where XAI guidance enhances focus and thus improves reliability.

It is possible for a network to make correct predictions based on irrelevant regions of the ECG signals. Therefore, it is important to assess the focusing areas in the ECG signal by the network. To evaluate the trustworthiness of our proposed network, we used Grad-CAM to determine which parts of the signal the network focuses on.

Figure 3 illustrates the effectiveness of XAI guidance. The left side shows CAMs without XAI guidance, while the right side presents CAMs with XAI guidance applied. In sample (a), the left CAM highlights some incorrect regions that contributed to the prediction. In contrast, the right CAM, utilizing XAI guidance, displays improved focus and reliability. Although the network correctly identified the arrhythmia in both cases, XAI guidance enhanced the trustworthiness of the results.

A similar scenario is observed in sample (e), where the left CAM indicates that the network did not focus on the most critical features of the ECG signal. In contrast, with XAI guidance, the model learns to concentrate on the relevant areas that cardiologists typically consider when making decisions. Thus, Figure 3 clearly illustrates the qualitative impact of XAI guidance and underscores its importance in achieving reliable predictions.

4.3 Limitations and future works

Our proposed network shows reliable and promising results when compared with state-of-the-art approaches. It is not without limitations, though. First, the number of

quantitative features trained could be expanded to allow the model to learn more statistical characteristics. Second, we relied solely on Grad-CAM for XAI guidance due to its simplicity. While effective, other advanced CAM-generating techniques might enhance the network’s ability to focus on critical features of the ECG signal.

This work serves as an initial exploration of the positive effects of XAI guidance in ECG arrhythmia classification. Furthermore, we limited our ground truth generation for XAI guidance to RR intervals variability for the sake of simplicity and automation. However, complex arrhythmias also involve other important features, such as P waves absence, ST elevation, and T waves position. Including these would require manual identification of the affected regions, necessitating collaboration with expert cardiologists and additional labor time. Thus, addressing these limitations will be a central focus of our future work.

5 Conclusion

In this paper, we proposed EXGnet, a single-lead XAI guided network designed for trustworthy ECG arrhythmia classification. We introduced a multiresolution feature extraction method that reduces computational demands while maintaining performance. By employing Grad-CAM based XAI guidance alongside train-only quantitative features, we aimed to enhance the model’s performance and trustworthiness. Our findings demonstrate that XAI guidance significantly improves the network’s ability to detect arrhythmias from true abnormal regions in the ECG signal. While the machine learning features contribute positively, they are not necessary during testing primarily; however, their inclusion during testing leads to a notable performance increase. According to the experimental results, EXGnet outperforms recent state-of-the-art networks across all metrics. Overall, our investigation confirms that this technique is not only effective but also reliable, making it well-suited for practical applications in portable single-lead ECG devices and beyond.

Acknowledgements

We would like to express our gratitude to Teton Private Ltd. for their partial financial support in conducting this project.

Author contributions

Tushar Talukder Showrav: Original draft preparation, Methodology, Software, Validation, Investigation, Visualization. Soyabul Islam Lincoln: Original draft preparation, Software, Validation, Investigation. Md. Kamrul Hasan: Data curation, Conceptualization, Supervision, Writing – review & editing.

Funding

The authors received no specific funding for this study.

Availability of data and materials

We used two public datasets in this work. Both of these datasets are jointly available online in a Physionet official link (<https://physionet.org/content/ecg-arrhythmia/1.0.0/>).

Ethics approval and consent to participate

Not applicable.

Consent for publication

Not applicable.

Competing Interests

The authors declare that there are no competing interests.

References

- [1] World Health Organization: Cardiovascular diseases Report 2022. https://www.who.int/health-topics/cardiovascular-diseases#tab=tab_1. Accessed: [September, 2024]
- [2] Repositioning of the global epicentre of non-optimal cholesterol. *Nature* **582**(7810), 73–77 (2020)
- [3] A B M Abdullah: ECG in Medical Practice, 5th edn. Jaypee Brothers Medical Publishers, New Delhi, India (2022). Chapter-1, Page: 7-10
- [4] Islam, M.S., Hasan, K.F., Sultana, S., Uddin, S., Quinn, J.M., Moni, M.A., *et al.*: Hardc: A novel ecg-based heartbeat classification method to detect arrhythmia using hierarchical attention based dual structured rnn with dilated cnn. *Neural Networks* **162**, 271–287 (2023)
- [5] Ye, C., Kumar, B.V., Coimbra, M.T.: Heartbeat classification using morphological and dynamic features of ecg signals. *IEEE Transactions on Biomedical Engineering* **59**(10), 2930–2941 (2012)
- [6] Kutlu, Y., Kuntalp, D.: Feature extraction for ecg heartbeats using higher order statistics of wpd coefficients. *Computer Methods and Programs in Biomedicine* **105**(3), 257–267 (2012)
- [7] Chen, S., Hua, W., Li, Z., Li, J., Gao, X.: Heartbeat classification using projected and dynamic features of ecg signal. *Biomedical Signal Processing and Control* **31**, 165–173 (2017)

- [8] Shi, H., Wang, H., Huang, Y., Zhao, L., Qin, C., Liu, C.: A hierarchical method based on weighted extreme gradient boosting in eeg heartbeat classification. *Computer Methods and Programs in Biomedicine* **171**, 1–10 (2019)
- [9] Yang, H., Wei, Z.: Arrhythmia recognition and classification using combined parametric and visual pattern features of eeg morphology. *IEEE Access* **8**, 47103–47117 (2020)
- [10] Mihandoost, S., Amirani, M.C.: Cyclic spectral analysis of electrocardiogram signals based on garch model. *Biomedical Signal Processing and Control* **31**, 79–88 (2017)
- [11] Hannun, A.Y., Rajpurkar, P., Haghpanahi, M., Tison, G.H., Bourn, C., Turakhia, M.P., Ng, A.Y.: Cardiologist-level arrhythmia detection and classification in ambulatory electrocardiograms using a deep neural network. *Nature Medicine* **25**(1), 65–69 (2019)
- [12] Petmezas, G., Haris, K., Stefanopoulos, L., Kilintzis, V., Tzavelis, A., Rogers, J.A., Katsaggelos, A.K., Maglaveras, N.: Automated atrial fibrillation detection using a hybrid cnn-lstm network on imbalanced eeg datasets. *Biomedical Signal Processing and Control* **63**, 102194 (2021)
- [13] Guan, Y., An, Y., Xu, J., Liu, N., Wang, J.: Ha-resnet: Residual neural network with hidden attention for eeg arrhythmia detection using two-dimensional signal. *IEEE/ACM Transactions on Computational Biology and Bioinformatics* **20**(6), 3389–3398 (2022)
- [14] Serhal, H., Abdallah, N., Marion, J.-M., Chauvet, P., Oueidat, M., Humeau-Heurtier, A.: An emd-based approach for atrial fibrillation classification using wavelets and convolutional neural network. *Biomedical Signal Processing and Control* **82**, 104507 (2023)
- [15] Hao, S., Xu, H., Ji, H., Wang, Z., Zhao, L., Ji, Z., Ganchev, I.: G2-resnext: a novel model for eeg signal classification. *IEEE Access* **11**, 34808–34820 (2023)
- [16] Xie, J., Stavrakis, S., Yao, B.: Automated identification of atrial fibrillation from single-lead eegs using multi-branching resnet. *Frontiers in Physiology* **15**, 1362185 (2024)
- [17] Singhal, S., Kumar, M.: Gsm-d-srst: Group sparse mode decomposition and superlet transform based technique for multi-level classification of cardiac arrhythmia. *IEEE Sensors Journal* (2024)
- [18] El-Ghaish, H., Eldele, E.: Eegtransform: Empowering adaptive eeg arrhythmia classification framework with bidirectional transformer. *Biomedical Signal Processing and Control* **89**, 105714 (2024)

- [19] Choi, S., Choi, K., Yun, H.K., Kim, S.H., Choi, H.-H., Park, Y.-S., Joo, S.: Diagnosis of atrial fibrillation based on ai-detected anomalies of ecg segments. *Heliyon* **10**(1) (2024)
- [20] Chen, J., Fang, B., Li, H., Zhang, L.-b., Teng, Y., Fortino, G.: Emcnet: Ensemble multiscale convolutional neural network for single-lead ecg classification in wearable devices. *IEEE Sensors Journal* (2024)
- [21] Goettling, M., Hammer, A., Malberg, H., Schmidt, M.: xecgarch: a trustworthy deep learning architecture for interpretable ecg analysis considering short-term and long-term features. *Scientific Reports* **14**(1), 13122 (2024)
- [22] Ayano, Y.M., Schwenker, F., Dufera, B.D., Debelee, T.G., Ejegu, Y.G.: Interpretable hybrid multichannel deep learning model for heart disease classification using 12-leads ecg signal. *IEEE Access* (2024)
- [23] Asgharzadeh-Bonab, A., Amirani, M.C., Mehri, A.: Spectral entropy and deep convolutional neural network for ecg beat classification. *Biocybernetics and Biomedical Engineering* **40**(2), 691–700 (2020)
- [24] Meng, L., Tan, W., Ma, J., Wang, R., Yin, X., Zhang, Y.: Enhancing dynamic ecg heartbeat classification with lightweight transformer model. *Artificial Intelligence in Medicine* **124**, 102236 (2022)
- [25] Tao, Y., Li, Z., Gu, C., Jiang, B., Zhang, Y.: Ecg-based expert-knowledge attention network to tachyarrhythmia recognition. *Biomedical Signal Processing and Control* **76**, 103649 (2022)
- [26] Bechinia, H., Benmerzoug, D., Khelifa, N.: Approach based lightweight custom convolutional neural network and fine-tuned mobilenet-v2 for ecg arrhythmia signals classification. *IEEE Access* **12**, 40827–40841 (2024)
- [27] Islam, M.R., Qaraqe, M., Qaraqe, K., Serpedin, E.: Cat-net: Convolution, attention, and transformer based network for single-lead ecg arrhythmia classification. *Biomedical Signal Processing and Control* **93**, 106211 (2024)
- [28] Jo, Y.-Y., Cho, Y., Lee, S.Y., Kwon, J.-m., Kim, K.-H., Jeon, K.-H., Cho, S., Park, J., Oh, B.-H.: Explainable artificial intelligence to detect atrial fibrillation using electrocardiogram. *International Journal of Cardiology* **328**, 104–110 (2021)
- [29] Bender, T., Beinecke, J.M., Krefting, D., Müller, C., Dathe, H., Seidler, T., Spicher, N., Hauschild, A.-C.: Analysis of a deep learning model for 12-lead ecg classification reveals learned features similar to diagnostic criteria. *IEEE Journal of Biomedical and Health Informatics* **28**(4), 1848–1859 (2023)
- [30] Singh, P., Sharma, A.: Interpretation and classification of arrhythmia using deep convolutional network. *IEEE Transactions on Instrumentation and Measurement*

- [31] Le, K.H., Pham, H.H., Nguyen, T.B., Nguyen, T.A., Thanh, T.N., Do, C.D.: Lightx3ecg: A lightweight and explainable deep learning system for 3-lead electrocardiogram classification. *Biomedical Signal Processing and Control* **85**, 104963 (2023)
- [32] Reyna, M.A., Sadr, N., Alday, E.A.P., Gu, A., Shah, A.J., Robichaux, C., Rad, A.B., Elola, A., Seyedi, S., Ansari, S., *et al.*: Will two do? varying dimensions in electrocardiography: the physionet/computing in cardiology challenge 2021. In: 2021 Computing in Cardiology (CinC), vol. 48, pp. 1–4 (2021). IEEE
- [33] Zheng, J., Zhang, J., Danioko, S., Yao, H., Guo, H., Rakovski, C.: A 12-lead electrocardiogram database for arrhythmia research covering more than 10,000 patients. *Scientific data* **7**(1), 48 (2020)
- [34] Zheng, J., Chu, H., Struppa, D., Zhang, J., Yacoub, S.M., El-Askary, H., Chang, A., Ehwerhemuepha, L., Abudayyeh, I., Barrett, A., *et al.*: Optimal multi-stage arrhythmia classification approach. *Scientific reports* **10**(1), 2898 (2020)
- [35] Ribeiro, E., Soares, Q.B., Dias, F.M., Krieger, J.E., Gutierrez, M.A.: Can deep learning models differentiate atrial fibrillation from atrial flutter? medRxiv, 2023–08 (2023)
- [36] Makowski, D., Pham, T., Lau, Z.J., Brammer, J.C., Lespinasse, F., Pham, H., Schölzel, C., Chen, S.H.A.: NeuroKit2: A python toolbox for neurophysiological signal processing. *Behavior Research Methods* **53**(4), 1689–1696 (2021) <https://doi.org/10.3758/s13428-020-01516-y>
- [37] Ibtehaz, N., Rahman, M.S.: Multiresunet: Rethinking the u-net architecture for multimodal biomedical image segmentation. *Neural Networks* **121**, 74–87 (2020)
- [38] Showrav, T.T., Hasan, M.K.: Hi-gmisnet: generalized medical image segmentation using dwt based multilayer fusion and dual mode attention into high resolution pgan. *Physics in Medicine & Biology* **69**(11), 115019 (2024)
- [39] Selvaraju, R.R., Cogswell, M., Das, A., Vedantam, R., Parikh, D., Batra, D.: Grad-cam: Visual explanations from deep networks via gradient-based localization. In: *Proceedings of the IEEE International Conference on Computer Vision*, pp. 618–626 (2017)
- [40] Peltola, M.A.: Role of editing of r-r intervals in the analysis of heart rate variability. *Frontiers in physiology* **3**, 148 (2012)